Quasi Steady-State Modeling and Characterization of Diffusion-Controlled Dissolution from Polydisperse Spheroidal Particles, II: Characterization

Yanxing Wang[1,*], Hui Wan[2], Cody Barka[1], Tie Wei[3], and Fangjun Shu[1],

[1]*Department of Mechanical and Aerospace Engineering, New Mexico State University, Las Cruces, NM 88003, USA*

[2]*Department of Mechanical and Aerospace Engineering, University of Colorado, Colorado Springs, CO 80918, USA*

[3]*Department of Mechanical Engineering, New Mexico Institute of Mining and Technology, Socorro, NM 87801, USA*

A quasi steady-state model (QSM) for accurately predicting the detailed diffusion-dominated dissolution process of polydisperse spheroidal (prolate, oblate, and spherical) particle systems was presented Part I of this study. In the present paper, the dissolution characteristics of typical polydisperse spheroidal particle systems have been extensively investigated. The effects of the distributions of particle size and shape have been studied by examining the detailed dissolution processes, such as the size reduction rates of individual particles, the increase in bulk concentration, and the dissolution time of the polydisperse systems. Some important factors controlling the dissolution process, including initial particle concentration, smallest and largest particle sizes, and the smallest and largest Taylor shape parameters, have been identified.

1. Introduction

The modeling and characterization of dissolution processes in polydisperse particle systems are of great importance to many scientific and industrial applications, such as drug delivery [1], metal ore heap leaching [2], renewable biomass energy [3], and dissolvable microrobots [4]. A full understanding of the dissolution kinetics is vital to uncovering the underlying physical and chemical mechanism involved [5].

The dissolution process relies on both molecular diffusion and the hydrodynamics around the particle. In many applications, such as drug dissolution in the gastrointestinal tract, the particle sizes range from a few microns to hundreds of microns [6,7]. For such small particles, hydrodynamic effect is relatively weak and molecular diffusion plays a dominant role in mass transfer [8]. To date, a large number of diffusion-dominated dissolution models have been developed and widely applied in various areas [9-19]. These models typically incorporate a parameter known as diffusion layer thickness, which is based on the recognition that a layer of high concentration fluid exists adjacent to the particle surface [9,14]. These models have been shown to accurately predict the entire dissolution process of spherical particles, but they are generally empirical or semi-empirical, lacking rigorous mathematical proof, and having limited applicability. In nature and practical applications, more than 70% of solid particles are not regularly spherical, and have a wide range of aspect ratio from $O(0.1)$ to $O(10)$ [20, 21]. Morphology has been identified as a key factor influencing the dissolution process [1, 20, 21]. Nevertheless, most existing models cannot appropriately handle the non-spherical particles. They usually apply a spherical-particle-based model and introduce a shape factor as an empirical correction, devoid of rigorous mathematical substantiation[22, 23]. These major modeling limitations have hindered the accurate prediction on the polydisperse dissolution of non-spherical particles and, consequently, a comprehensive understanding of the underlying dissolution mechanisms remains elusive.

*yxwang@nmsu.edu

Understanding the dissolution process of spheroidal particles, including prolate, oblate, and spherical shapes, is a significant stride in revealing the dissolution mechanisms of non-spherical particles. Wang et al. [24] extended the Quasi-Steady-State Model (QSM) for spherical particles to include prolate and oblate spheroidal particles, employing analytical solutions to the steady-state diffusion equation in spheroidal coordinate systems. This extension enables the examination of detailed dissolution characteristics, including the molar flux of dissolved substances and the regression rate of the particle surface, based on the spatial distribution of molar concentration in the surrounding fluid. This model of a single spheroidal particle establishes the crucial foundation for subsequent polydisperse dissolution models.

In Part I of this study [25], we integrated a rigorous mathematically-based QSM model for diffusion-dominated dissolution of single spheroidal (prolate, oblate, or spherical) particles into the well-established framework of polydisperse dissolution models, and developed a mathematical model that can accurately predict the detailed dissolution process in systems of spheroidal particles with a broad particle size and aspect ratio distributions. Verification against experimental results shows that this model can accurately predict the increase in bulk concentration of polydisperse systems with various particle sizes and shape parameters. In Part II, we leverage this model to systematically investigate the dissolution of polydisperse systems, aiming to identify the effects of particle size and shape distribution, as well as the initial particle concentration, on detailed dissolution processes such as individual particle size reduction, bulk concentration increase, and overall dissolution time of the entire polydisperse systems.

2. Research design

To identify the dissolution physics, we use the parameters of a commonly-used drug for hypertension, felodipine. The molar volume of felodipine is $v_m = 265$ cm^3/mol. The solubility of felodipine in water is $C_{sol} = 0.89$ μM, which is also the saturation concentration (C_s). The diffusion coefficient of felodipine is $D_m = 6.7 \times 10^{-6}$ cm^2/s [26].

In this study, we consider a polydisperse system with continuous distributions of size and aspect ratio of spheroidal particles. In fields such as pharmacology and crystallography, the log-normal distribution has been used for a long time to describe the size distribution of particles; the particle distribution is described as a normal or Gaussian function on a logarithm scale of particle size [27, 28]. The volumetric probability distribution function (PDF) of particle size with respect to the logarithm of equivalent spherical particle radius is defined as,

$$P^v_{logR}(logR,t)\delta(logR) = \frac{\delta(V_p(t))_{logR\to logR+\delta(logR)}}{V_p(t)} \tag{1}$$

and

$$\int_{logR_{min}}^{logR_{max}} P^v_{logR}(logR,t)d(logR) = 1 \tag{2}$$

where $P^v_{logR}(t)$ is the volumetric PDF of particle size at time t, $\delta(V_p(t))_{logR\to logR+\delta(logR)}$ is the particle volume in the range from $logR$ to $logR + \delta(logR)$, $V_p(t)$ is the total particle volume, and R_{min} and R_{max} are the minimum and maximum particle radius, respectively. The log-normal form of the volumetric PDF of particle size with respect to $logR$ at $t = 0$ is given as,

$$P^v_{logR,0}(logR) = \frac{1}{\sqrt{2\pi\sigma^2}} exp\left[-\frac{(logR-logR^*)^2}{2\sigma^2}\right] \tag{3}$$

where σ is the standard deviation of the distribution, and R^* is the particle radius at which the maximum $P^v_{logR,0}$ is reached. Based on R^*, we define a dissolution time scale, τ_{diss}, which is the time scale required for a spherical particle with radius R^* to fully dissolve at zero bulk concentration,

$$\tau_{diss} = \frac{R^{*2}}{2v_m C_s D_m} \tag{4}$$

τ_{diss} will be used to normalize time t in the following analysis.

In this study, we consider a narrow distribution with $\sigma^2 = 0.02$ and a wide distribution with $\sigma^2 = 0.18$. Two initial distributions start at a minimum particle radius and end at a maximum radius. The minimum and maximum particle sizes are selected so as to make

$$\left(P^v_{logR,0}\right)_{R=R_{0,min}} / \left(P^v_{logR,0}\right)_{R=R^*} = \left(P^v_{logR,0}\right)_{R=R_{0,max}} / \left(P^v_{logR,0}\right)_{R=R^*} = 0.01 \tag{5}$$

Here $R_{0,min}$ and $R_{0,max}$ are the minimum and maximum particle radii at $t = 0$, respectively. It can be calculated that for the narrow distribution,

$$\left(R_{0,min}/R^*\right)_{narrow} = 0.65 \quad \text{and} \quad \left(R_{0,max}/R^*\right)_{narrow} = 1.54 \tag{6}$$

and for the wide distribution,

$$\left(R_{0,min}/R^*\right)_{wide} = 0.28 \quad \text{and} \quad \left(R_{0,max}/R^*\right)_{wide} = 3.62 \tag{7}$$

The distribution is symmetric about $logR^*$. Figure 1 shows the initial profile of $P^v_{logR,0}$ of the narrow and wide distributions that will be investigated in this study. Obviously, the particle sizes in the narrow distribution are more uniform than in the wide distribution. Thus, the dissolution characteristics of the narrow distribution are between those of the monodisperse and wide distribution.

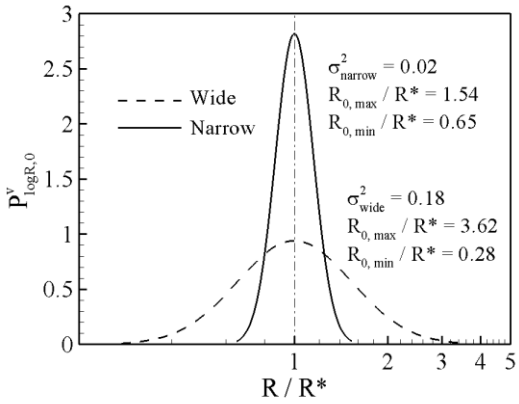

Figure 1. Initial narrow and wide particle size distributions considered in this study.

In the polydisperse system considered in this study, the aspect ratio of the spheroidal particles continuously ranges from $1/10$ for prolate particles to 10 for oblate particles in the initial distribution of Λ. The Taylor deformation parameter, D, is used instead of Λ to define the PDF. The relationship between D and Λ is,

$$D = \frac{\Lambda - 1}{\Lambda + 1} \tag{8}$$

When $\Lambda = 1/10$, $D = -9/11$, and when $\Lambda = 10$, $D = 9/11$. For spherical particles, $D = 0$. The width of the range of D of prolate particles ($D < 0$) is equal to that of oblate particles ($D > 0$).

The volumetric PDF in the space of $logR$ and D, which is denoted by $P^v_{logR,D}(logR, D, t)$, is defined as,

$$P^v_{logR,D}(logR, D, t)\delta(logR)\delta D = \frac{\delta\left(V_p(t)\right)_{logR \to logR+\delta(logR), D \to D+\delta D}}{V_p(t)} \tag{9}$$

where $\delta(V_p(t))_{logR \to logR+\delta(logR),D \to D+\delta D}$ is the particle volume in the range from $logR$ to $logR + \delta(logR)$ and from D to $D + \delta D$, $D_{max} = 9/11$ and $D_{min} = -9/11$. Based on the definition, we have the following relationship,

$$\int_{D_{min}}^{D_{max}} P^v_{logR,D}(logR, D, t) dD = P^v_{logR}(logR, t) \tag{10}$$

To simplify the problem, we assume that at $t = 0$, $P^v_{logR,D,0}$ is uniform over D from $9/11$ to $9/11$ for any $logR$,

$$P^v_{logR,D,0}(logR, D) = P^v_{logR,0}(logR)/(D_{max} - D_{min}) \tag{11}$$

and $P^v_{logR,0}(logR)$ is described by a log-normal function given by Eqn. (3). $P^v_{logR,D,0}$ is finally written as,

$$P^v_{logR,D,0}(logR, D) = \frac{1}{\sqrt{2\pi\sigma^2}} exp\left[-\frac{(logR - logR^*)^2}{2\sigma^2}\right]/(D_{max} - D_{min}) \tag{12}$$

For systems with a uniform particle size, the volumetric PDF with respect to Taylor shape parameter $P^v_D(t)$ is defined as,

$$P^v_D(D, t)\delta D = \frac{\delta(V_p(t))_{D \to D+\delta D}}{V_p(t)} \tag{13}$$

where $\delta(V_p(t))_{D \to D+\delta D}$ is the particle volume in the range from D to $D + \delta D$. When $t = 0$,

$$P^v_{D,0}(D) = \frac{1}{(D_{max} - D_{min})} \tag{14}$$

For the details of the implementation of the polydisperse model, please see Wang et al. [25].

2. Analysis of Dissolution Process

(a) Effect of initial particle size distribution for a given shape factor

In a polydisperse particle system, the size reduction rate and mass release rate of particles of different sizes and shapes are different, so the time variation of bulk concentration is different from that of the monodisperse system. We first examine the effect of particle size distribution on the polydisperse particle dissolution. In order to do this, we construct several polydisperse spheroidal particle systems, in which the particle size follows the narrow and wide distributions shown in Fig. 1. In each system, all the particles have the same shape, which is represented by the Taylor shape factor D. Three typical particle shapes with $D = -9/11$, 0 and 9/11 are selected, corresponding to a prolate, a spherical, and an oblate particle, respectively. The purpose is to find out the general effect of particle size distribution with different particle shapes. We use three representative initial particle concentrations, $C_{p,0}/C_s = 0.1$, 1, and 10, to study the detailed dissolution process under various conditions, corresponding to scenarios where particles completely dissolve, particles completely dissolve and the solution is saturated, and particles partially dissolve and the solution is saturated.

We begin the analysis with three cases with Taylor shape factors $D = -9/11$, 0, and 9/11, respectively, a narrow particle size distribution, and an initial particle concentration of $C_{p,0}/C_s = 0.1$. It is shown in Fig. S1 of supplementary materials that the particle sizes all decrease following a similar pattern. For the same initial size, the radius reduction rate, $|d(R/R^*)/d(t/\tau_{diss})|$, of non-spherical particles ($D = -9/11$ and

9/11) is larger than that of spherical particles (D =0). This has been discussed in Wang et al. [24]. For any given particle, the reduction rate, $|d(R/R^*)/d(t/\tau_{diss})|$, increases with decrease in (R/R^*), and approaches infinity when (R/R^*) goes to 0. For the same particle shape, that is, the same D, the reduction rate of smaller particles is larger than that of larger particles at the same t/τ_{diss}. These two phenomena are related to the dependence of particle size reduction rate on particle radius. In a polydisperse system, the mass release rate at the particle surface for both spherical and non-spherical particles can be written in a unified form as,

$$N'_{S,i} = -4\pi R^2 D_m \frac{(C_s - C_b)}{\delta_i(t)} \tag{15}$$

According to [24] and [29], $\delta_i(t)$ is linearly proportional to the equivalent spherical radius, with the proportional factor being a function of particle shape,

$$\delta_i(t) = f(D)R \tag{16}$$

where $f(D)$ is a function of the Taylor shape parameter of the particle. From the discussion in Wang et al. [24] it is known that $f(D) < 1$ for spheroidal particles, and $f(D)$ increases with increase in D when $D < 0$ and decreases with increase in D when $D > 0$. Substituting Eqns. (15) and (16) into the equation for particle radius reduction rate, Eqn. (14) in Part I [25], yields

$$\frac{dR}{dt} = -\frac{D_m(C_s - C_b)v_m}{f(D)R} \tag{17}$$

Therefore, for the same C_b, the magnitude of dR/dt is inversely proportional to R. For a given particle, the effect of increasing C_b on $|dR/dt|$ is overridden by the effect of decreasing R when $C_{p,0}/C_s = 0.1$.

The particle size reduction in a polydisperse system will lead to change in the volumetric PDF of particle size, that is, $P^v_{logR}(t)$. In Fig. 2 we show the time evolution of the profiles of $P^v_{logR}(t)$ against R/R^* for the cases of $D = -9/11$, 0 and 9/11 with a narrow initial distribution and an initial particle concentration $C_{p,0}/C_s = 0.1$. As the figure shows, the profiles of $P^v_{logR}(t)$ of the three cases evolve in a similar pattern, yet with an obvious difference in the rate of evolution. Throughout the evolution all of the particles decrease continuously in size, which causes the profile to shift in the direction of small particle size. Since the size reduction rate $|dR/dt|$ of the smaller particles is larger than that of larger particles, the profile gradually becomes wider, and the peak of the profile becomes lower. Due to the faster size reduction rate, smaller particles of the same volume lose volume faster than larger particles, which makes the peak of the profile move towards the largest particles. After some time, the peak reaches the largest particles and the largest particles acquire the maximum P^v_{logR} in the profile. Since the smaller particles lose volume at a faster rate, the volume fraction of larger particles increases with time, and P^v_{logR} of the largest particles increases as the particles decrease in size. Compared with spherical particles ($D = 0$), prolate and oblate particles ($D = -9/11$ and 9/11) of the same size dissolve faster, so the profiles of $P^v_{logR}(t)$ evolve faster, as shown in the figure.

Equations (15) - (17) suggest that a smaller particle has a larger size reduction rate than a larger particle in the same container. It is important, therefore, to consider the contribution of particles of different sizes to the overall increase of bulk concentration C_b. Hence, we define a PDF of mass release rate in terms of particle size for systems of particles with the same shape,

$$P^N_{logR}(t)\delta(logR) = \frac{\delta(N'_S)_{logR \to logR+\delta(logR)}}{N'_{S,tot}(t)} \tag{18}$$

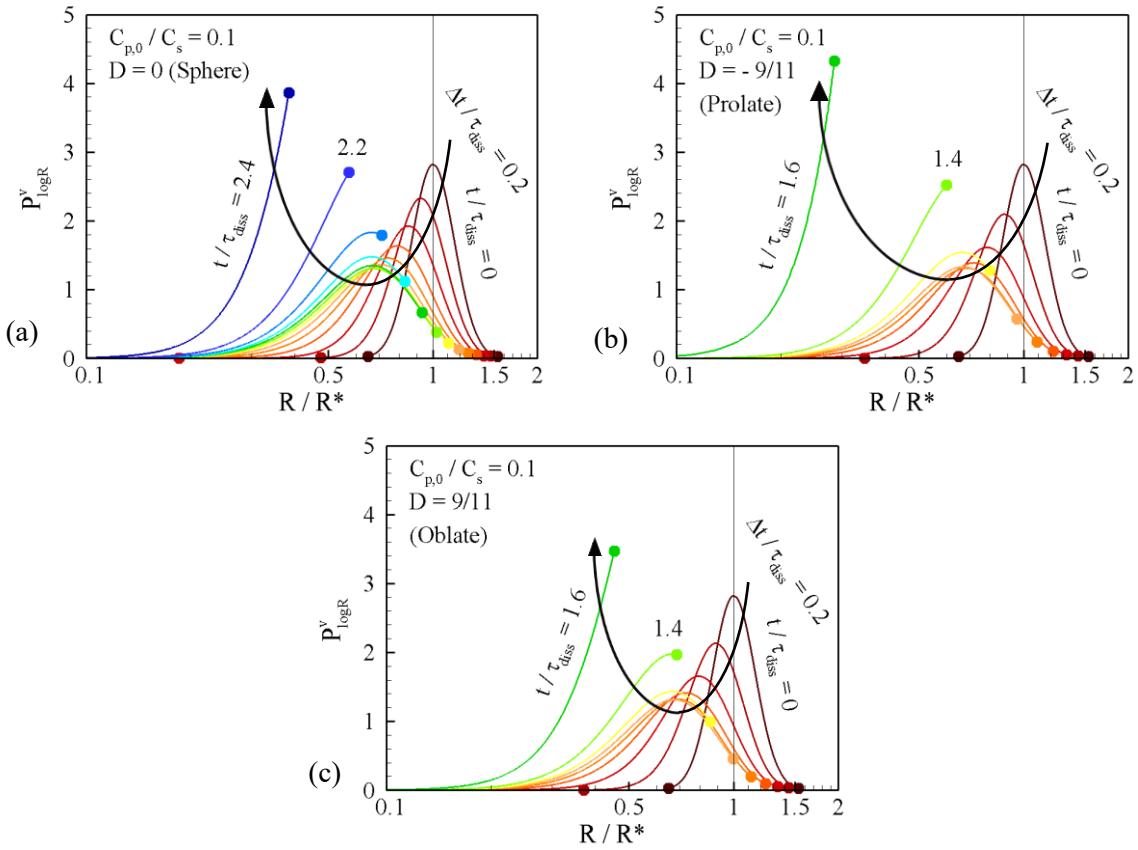

Figure 2. Evolution of particle size distribution (P^{v}_{logR}) with a narrow initial distribution for a given aspect ratio for $C_{p,0}/C_s = 0.1$. (a) spherical ($D = 0$), (b) prolate ($D = -9/11$), and (c) ($D = 9/11$). The solid dots indicate the smallest and largest particles in each distribution.

where $\delta(N'_S)_{logR \to logR+\delta(logR)}$ is the mass release rate from particles in the range from $logR$ to $logR + \delta(logR)$, and $N'_{S,tot}(t)$ is the total mass release rate from all particles in the system. It is shown in Fig. S2 of supplementary materials that smaller particles have a larger P^{N}_{logR} than larger particles of the same P^{v}_{logR}. In a broader sense, an unweighted dissolution rate of particles of a certain size can be defined as the total dissolution rate of a reference volume of particles of this size,

$$M'_S(R) = \frac{V_{ref}}{\frac{4}{3}\pi R^3} N'_{S,i} = -\frac{V_{ref}}{\frac{4}{3}\pi R^3} 4\pi R^2 D_m \frac{(C_s - C_b)}{f(D)R} = -3V_{ref} D_m \frac{(C_s - C_b)}{f(D)R^2} \qquad (19)$$

where V_{ref} is the reference volume, and $N'_{S,i}$ denotes the mass release rate of a single particle with a radius of R. Equation (19) suggests that in a polydisperse system, the smaller particles make a larger unweighted contribution to the total mass release rate.

Compared with a narrow distribution, a wide distribution has a smaller minimum particle size and a larger maximum size. Differences in particle size mean some differences in the dissolution process. Here we consider three systems with particles of the same shape in each system. The Taylor shape parameters of the three systems are $D = -9/11$, 0, and 9/11, respectively. The particle size distributions in these systems

follow the wide distribution shown in Fig. 1. The initial concentration of solid particles is $C_{p,0}/C_s = 0.1$. It is shown in Fig. S3 of Supplementary Materials that the particles decrease in size in a pattern similar to that of the particles in a narrow distribution, shown in Fig. S1. The sizes of non-spherical ($D = -9/11$ and 9/11) particles decrease faster than those of spherical particles ($D = 0$), and smaller particles decrease in size faster than larger particles of the same shape.

When the initial particle size distribution is changed from narrow to wide, the difference in particle size reduction rate between the smaller and larger particles is magnified, which leads to the differences in the evolution of volumetric PDF of particle size P^v_{logR}. In Fig. 3 we plot the time evolution of the profiles of $P^v_{logR}(t)$ against R/R^* for three cases of $D = -9/11$, 0 and 9/11 with a wide initial distribution and an initial particle concentration $C_{p,0}/C_s = 0.1$. The profiles of three different D of the wide distribution evolve in a similar pattern. Compared with the narrow distribution, the decrease in the minimum particle size and the increase in the maximum size in the initial distribution make the smaller particles dissolve at an even faster rate relative to the larger particles. As a result, the profile of P^v_{logR} shifts as a whole towards the larger particle side in the initial period of time ($t/\tau_{diss} \lesssim 6$ for $D = 0$). This trend is opposite that of the narrow distribution, in which the relatively uniform particle sizes make the profile of P^v_{logR} shift toward the smaller particle side. Due to the larger size reduction rate of smaller particles, the peak of the profile moves toward the largest particles, which also decrease in size. At a certain moment, the peak reaches the largest particles and then moves to the smaller particle side with the particle size reduction. The change of P^v_{logR} of the largest particles can be divided into stages. In the first stage, the faster size reduction rates of smaller

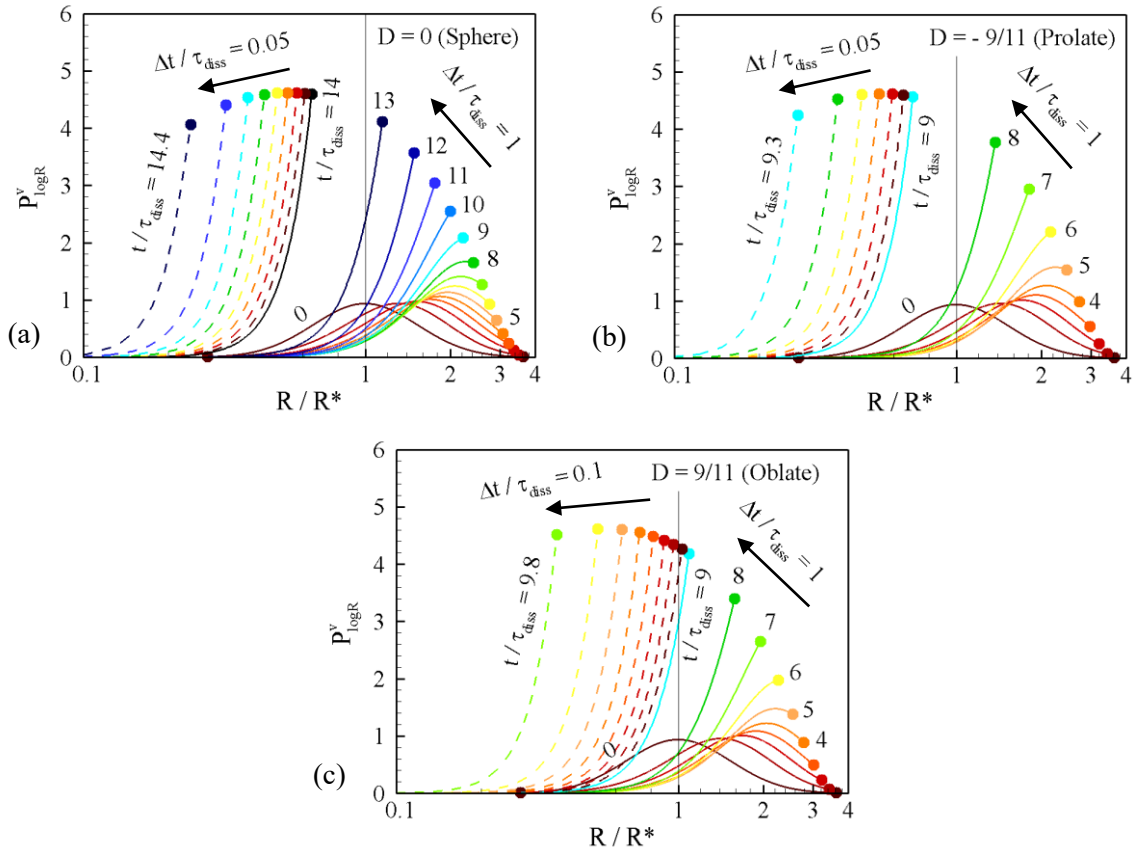

Figure 3. Evolution of particle size distribution (P^v_{logR}) with a wide initial distribution for a given aspect ratio for $C_{p,0}/C_s = 0.1$. (a) spherical ($D = 0$), (b) prolate ($D = -9/11$), and (c) ($D = 9/11$)

particles significantly increase the volume fraction of larger particles, so $(P_{logR}^{v})_{max}$ increases with time. After a critical time point (for example, $t/\tau_{diss} \approx 14\ for\ D = 0$), the scale of $logR$ is expanded as particle size approaches zero, which overrides the effect of increased volume fraction on P_{logR}^{v}. As a result, $(P_{logR}^{v})_{max}$ becomes decreasing with time. This phenomenon can also be observed in the dissolution process with a narrow initial distribution.

It is shown in Fig. S4 of Supplementary Materials that smaller particles make a larger contribution to the increase in bulk concentration than larger particles of the same P_{logR}^{v}, which is the same as that of a narrow distribution shown in Fig. S2.

When $C_{p,0}/C_s = 1$, that is, when the solid particles have completely dissolved and the solution is saturated, the dissolution exhibits different characteristics than at $C_{p,0}/C_s = 0.1$. According to Eqns. (15) and (17), when the bulk concentration C_b is close to 1, the mass release rate from the particle surface $N'_{S,i}$ and the particle size reduction rate dR/dt are close to 0. This makes it take an infinite amount of time for the particles to completely dissolve, which is theoretically impossible to actually achieve. This is confirmed by the variation of particle sizes in systems of spherical particles for $C_{p,0}/C_s = 1$, shown in Fig. S5 of Supplementary Materials. For both narrow and wide initial distributions, smaller particles, such as those with $R_0 = R^*$ and $R_{0,min}$, completely dissolve within a finite range of time, yet the complete dissolution of the largest particles cannot be achieved with a finite time. It has been shown in Figs. S1 and S3 that the dissolution process of non-spherical particles ($D \neq 0$) is similar to that of spherical particles ($D = 0$), so we only discuss the cases of spherical particles here. The corresponding evolution of volumetric particle size distribution, P_{logR}^{v}, are shown in Fig. 4. Since complete dissolution cannot be reached, we stopped the calculations when $C_b/C_s = 0.99$. That is, only 1% of the initial particle volume is left in the solution. Within this time range, the evolution of the profiles of P_{logR}^{v} demonstrates similar characteristics to the initial period of the case of $C_{p,0}/C_s = 0.1$. For the narrow distribution, the profile shifts towards the small particle side as a whole, accompanied by a broadening of the distribution and a decrease in the peak. For the wide distribution, the profile shifts towards the large particle side as a whole, accompanied by an increase in the peak. These phenomena are caused by the difference in particle size reduction rate in the distribution.

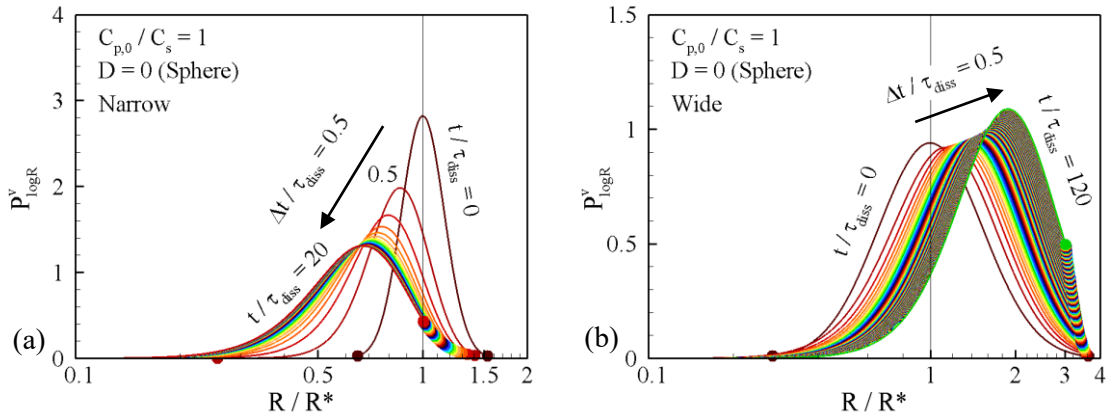

Figure 4. Evolution of particle size distribution (P_{logR}^{v}) of spherical particles for $C_{p,0}/C_s = 1$. (a) Narrow, and (b) wide initial distributions.

When $C_{p,0}/C_s = 10$, the fraction of solid particles exceeds that which is required to saturate the solution. 90% of the initial particle volume will be left at saturation. It is shown in Fig. S6 of Supplementary Materials that it takes an infinite amount of time to reach full saturation, so the calculations were stopped when $C_b/C_s = 0.99$. For both narrow and wide distributions, even the smallest particles do not completely dissolve. All particles asymptotically approach their respective final-state constant particle sizes. The corresponding evolution of volumetric particle size distribution, P^v_{logR}, is shown in Fig. 5. For this high initial particle concentration, the profiles of P^v_{logR} do not change very much from that of $t = 0$. The trend of slight changes is similar to the cases of $C_{p,0}/C_s = 1$, which are analyzed above.

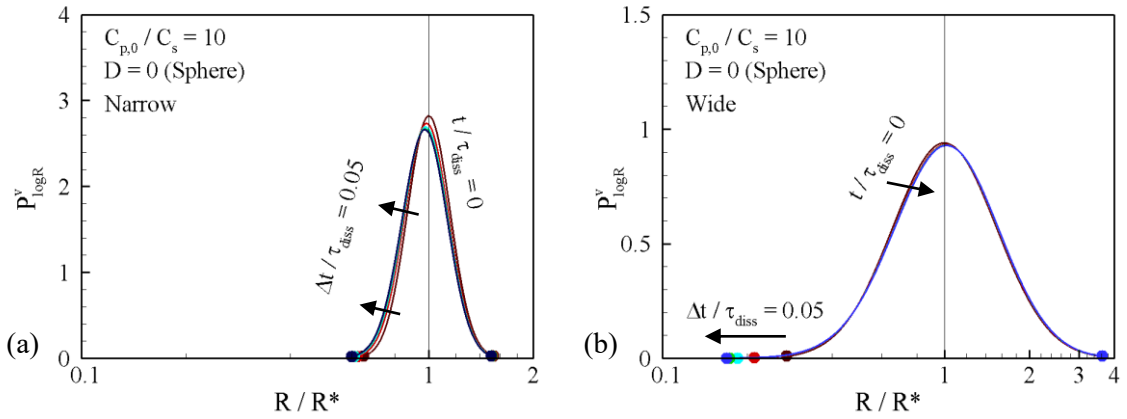

Figure 5. Evolution of particle size distribution (P^v_{logR}) of spherical particles for $C_{p,0}/C_s = 10$. (a) Narrow, and (b) wide initial distributions.

The nonuniform dissolution of polydisperse collections of particles discussed above result in different patterns of increase in the bulk concentration C_b. Here we only consider the systems with a wide initial particle size distribution, because of the prominent features caused by non-uniform dissolution, and compare the increase in C_b with those of monodisperse systems. In Fig. 6 we compare the variation of C_b with time (t/τ_{diss}) between polydisperse and monodisperse systems for prolate ($D = -9/11$), spherical ($D = 0$), and oblate ($D = 9/11$) particles. In each system the Taylor shape parameters are the same for all particles. Three initial particle concentrations, $C_{p,0}/C_s = 0.1$, 1 and 10 are considered. The difference in the increase of C_b among different particle shapes is discussed in Wang et al. [24]. Here we focus on the difference between polydisperse and monodisperse systems.

For the cases of $C_{p,0}/C_s = 0.1$ and 1, all particles will completely dissolve, given sufficient time. Figures 6(b) and (c) therefore exhibits similar trends of increase in C_b. In an initial short period, the nondimensional bulk concentrations C_b/C_s in polydisperse systems increase faster than those in monodisperse systems of the same particle shape (represented by Taylor shape parameter D). The reason is that the smaller particles in polydisperse systems have larger size reduction rates than particles in monodisperse systems, as shown in Eqn. (17). Under the condition of the same bulk concentration and the same volume of particles, the collection of smaller particles has a larger total mass release rate. This larger mass release rate of small particles makes the bulk concentration in polydisperse systems increase faster than in monodisperse systems. After the initial period, most of the small particles have dissolved, and the increase in C_b is primarily dominated by the dissolution of larger particles. The larger particles in polydisperse systems have smaller size reduction rates than particles in monodisperse systems (Eqn. (17)). As discussed above, the larger particles have a smaller mass release rate, which makes the bulk concentration in polydisperse systems increase slower than in monodisperse systems. At the same time, the

time required to completely dissolve the particles or reach $C_{p,0}/C_s = 0.99$ is significantly increased, as shown in the figure. When $C_{p,0}/C_s = 10$, the fraction of particles far exceeds that which would saturate the solution. The dissolution of the smaller particles in the polydisperse systems is sufficient to saturate the solution, so the time required for polydisperse systems to reach $C_{p,0}/C_s = 0.99$ is shorter than the time for monodisperse systems of the same particle shape, as shown in Fig. 6(d).

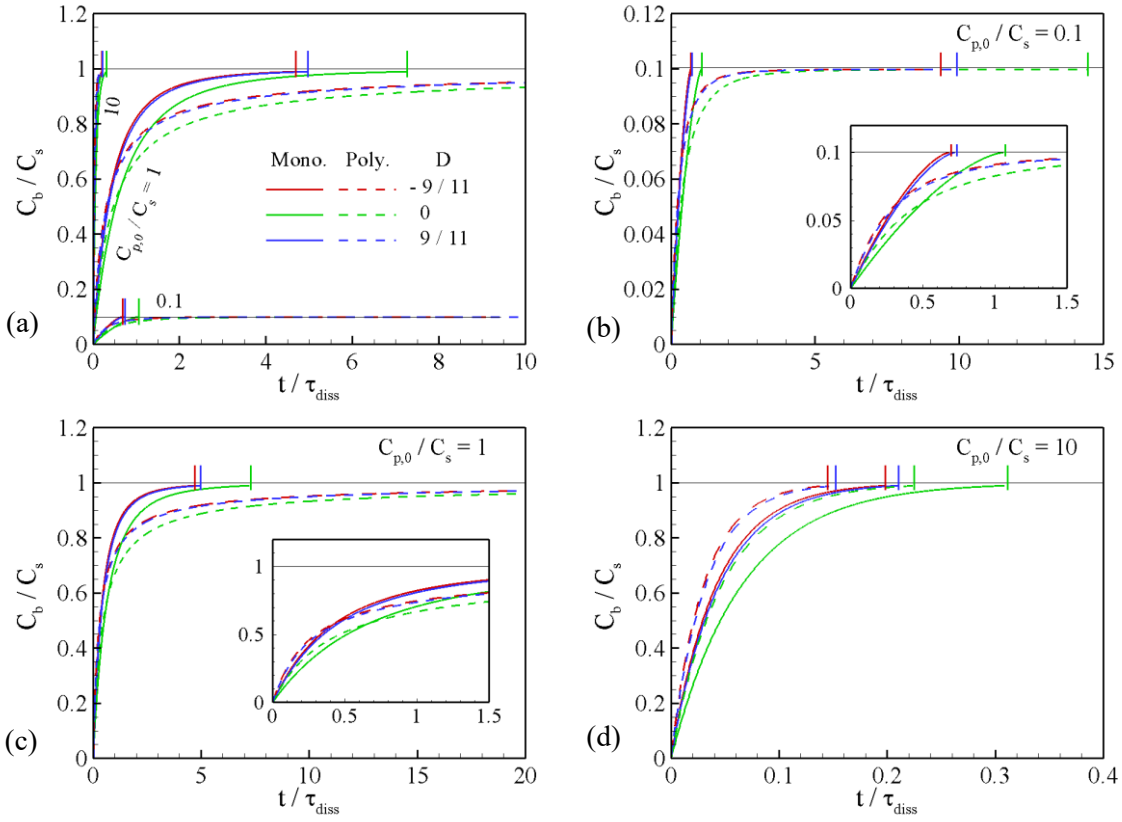

Figure 6 Variation of bulk concentration ($C_{p,0}/C_s$) with time (t/τ_{diss}) between monodisperse and polydisperse models for prolate ($D = -9/11$), spherical ($D = 0$) and oblate ($D = 9/11$) particles. (a) Three initial particle concentrations, $C_{p,0}/C_s = 0.1$, 1 and 10, (b) $C_{p,0}/C_s = 0.1$, (c) $C_{p,0}/C_s = 1$, (d) $C_{p,0}/C_s = 10$. The vertical lines indicate where the particles have completely dissolved or $C_b/C_s = 0.99$ is reached.

In addition to the bulk concentration C_b, the dissolution time of the systems is critical. Here we define the dissolution time (T) as the time required for all particles in a polydisperse system to completely dissolve when $C_{p,0}/C_s < 1$, or the time it takes for the bulk concentration (C_b/C_s) to reach 0.99 when $C_{p,0}/C_s \geq 1$. Figure 7 illustrates the normalized dissolution time T/τ_{diss} versus initial particle concentration $C_{p,0}/C_s$ for both monodisperse and polydisperse systems with narrow and wide distributions in the range from $C_{p,0}/C_s = 10^{-2}$ to 10^2. Within each system, all particles have the same Taylor shape parameter D. Three D are considered: $D = -9/11$, 0, and 9/11, corresponding to prolate, spherical, and oblate particles. As shown in the figure, a singular point with $T/\tau_{diss} \gg 1$ exists at $C_{p,0}/C_s = 1$. For every case, T/τ_{diss} monotonically increases with the increase in $C_{p,0}/C_s$ when $C_{p,0}/C_s < 1$, and monotonically decreases with the increase in $C_{p,0}/C_s$ when $C_{p,0}/C_s > 1$. According to the curve variation, four regimes of $C_{p,0}/C_s$ can be identified. In Regime I ($C_{p,0}/C_s < 10^{-1}$), the initial particle concentration ($C_{p,0}/C_s$) is small, which makes the bulk concentration (C_b/C_s) also low throughout the dissolution process. The dissolution time is

close to that of the largest particles of a system in an infinitely-large medium, since the dissolution of the largest particles is the limiting factor in the dissolution time of a polydisperse system. For a monodisperse system with spherical particles ($D = 0$), it is $T/\tau_{diss} = 1$. In this regime $log(T/\tau_{diss})$ is roughly constant for all cases. In Regime II ($10^{-1} < C_{p,0}/C_s \leq 1$), the effect of C_b appears, which reduces the dissolution rate and increases the dissolution time. As a result, $\log(T/\tau_{diss})$ increases with the increase in $\log(C_{p,0}/C_s)$, and reaches its maximum at $C_{p,0}/C_s = 1$. When $C_{p,0}/C_s > 1$, the solution is saturated in the end and $log(T/\tau_{diss})$ decreases with the increase in $\log(C_{p,0}/C_s)$, because of the increase in volume fraction of solid particles. In Regime III ($1 \leq C_{p,0}/C_s \leq 2$), $C_{p,0}/C_s$ is close to 1 and some nonlinear features due to non-uniform particle sizes are exhibited, so the curves are not straight. In Regime IV ($C_{p,0}/C_s > 2$), the curves demonstrate some linear features and $\log(T/\tau_{diss})$ changes roughly linearly with $\log(C_{p,0}/C_s)$. All curves have roughly the same slope, which is expected to be determined by the initial particle size distribution, as well as material properties such as $v_m C_s$. It should be pointed out that we only roughly divide the entire range of $C_{p,0}/C_s$ into four regimes based on the characteristics of curve variations. The locations of the boundaries between different regimes are not very strict and they should be adjusted according to the applications.

For all cases, $\log(T/\tau_{diss})$ of systems with spherical particles is larger than that of systems of non-spherical particles for each $\log(C_{p,0}/C_s)$. Wang et al. [24] showed that, for monodisperse systems, $\log(T/\tau_{diss})$ increases with increase in D when $D < 0$ (prolate particles), and $\log(T/\tau_{diss})$ decreases with increase in D when $D > 0$ (oblate particles). This conclusion is also valid for polydisperse systems.

The initial particle size distribution also plays a role in determining the dissolution time. When $C_{p,0}/C_s < 1$, the dissolution time T/τ_{diss} of a polydisperse system is limited by the dissolution of the largest particles. Since $(R_{0,max})_{wide} > (R_{0,max})_{narrow} > (R_{0,max})_{mono}$, where $(R_{0,max})_{wide}$, $(R_{0,max})_{narrow}$, and $(R_{0,max})_{mono}$ are the largest equivalent spherical radii in systems with wide, narrow, and monodisperse distributions, respectively, we have $(\log(T/\tau_{diss}))_{wide} > (\log(T/\tau_{diss}))_{narrow} > (\log(T/\tau_{diss}))_{mono}$ for the same D at any given $\log(C_{p,0}/C_s)$, as shown in the figure. When $C_{p,0}/C_s$ is slightly greater than 1, this relationship is still valid, because the largest particles still play an important role. However, further increase in $C_{p,0}/C_s$ changes the relationship. Since the smaller particles have larger size reduction rates, as shown by Eqn. (17), in the case of the same particle volume, the collection of smaller particles has a larger mass release rate, as shown by Eqn. (19). The increase in $C_{p,0}/C_s$ makes the volume of solid particles exceed that required to saturate the solution, thus reducing the volume fraction of larger particles dissolved into the solution. On the other hand, the increase in $C_{p,0}/C_s$ enhances the importance of the dissolution of smaller particles in the dissolution process. When $C_{p,0}/C_s$ is large enough, for example,

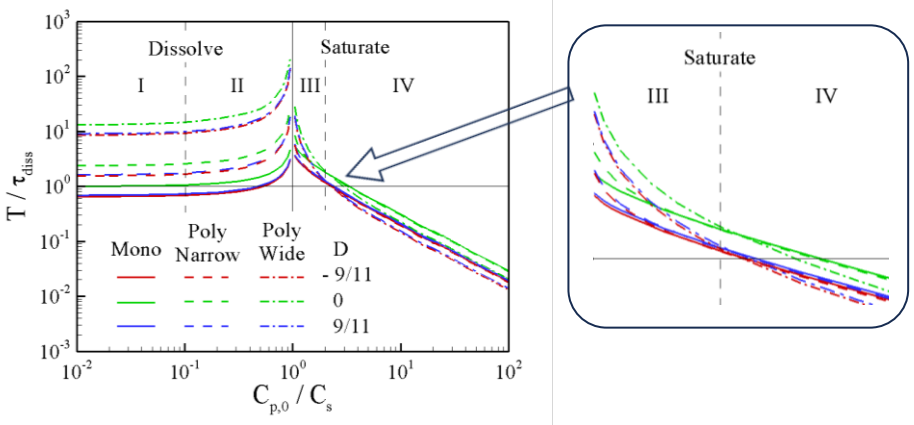

Figure 7. Variation of dissolution time (T/τ_{diss}) with initial concentration of solid particles ($C_{p,0}/C_s$) for monodisperse and polydisperse particles with given aspect ratios.

$C_{p,0}/C_s > 3$, the dissolution is primarily dominated by smaller particles in the systems. Since $(R_{0,min})_{wide} < (R_{0,min})_{narrow} < (R_{0,min})_{mono}$, where $(R_{0,min})_{wide}$, $(R_{0,min})_{narrow}$, and $(R_{0,min})_{mono}$, are the smallest equivalent spherical radii in systems with wide, narrow, and monodisperse distributions, respectively, $(\log(T/\tau_{diss}))_{wide} < (\log(T/\tau_{diss}))_{narrow} < (\log(T/\tau_{diss}))_{mono}$ for the same D at any given $\log(C_{p,0}/C_s)$, as shown in the figure.

From the above analysis, it can be seen that the particle size distribution causes a very complex dependence of the dissolution time (T/τ_{diss}) on the initial particle concentration $C_{p,0}/C_s$.

(b) Effect of Taylor shape parameter distribution with a same particle size

To study the effect of the Taylor shape parameter of spheroidal particles, we examine the dissolution processes of several systems with the same initial equivalent spherical radius $R_0 = R^*$ and a uniform initial volumetric PDF with respect to Taylor shape parameter, given by Eqn. (14). Here we consider three systems with initial particle concentrations $C_{p,0}/C_s = 0.1$, 1, and 10.

According to Eqn. (17), the particle size reduction rate, $|\,dR/dt\,|$, decreases with increase in D when $D < 0$, and increases with increase in D when $D > 0$, for a given C_b. Therefore, the equivalent spherical radius of non-spherical particles ($D = -9/11$ and 9/11) decreases faster than that of spherical particles ($D = 0$) for all $C_{p,0}/C_s$, as shown in Fig. S7 of Supplementary Materials. When $C_{p,0}/C_s = 0.1$, all particles completely dissolve. When $C_{p,0}/C_s = 10$, no particle completely dissolves and the solution is saturated in the end. When $C_{p,0}/C_s = 1$, the solution cannot be fully saturated within a finite range of time because of the decreased particle size reduction rate as C_b approaches C_s. Although most non-spherical particles completely dissolve, the spherical particles do not.

The particles of different D have different mass release and size reduction rates, and this causes different evolution of the PDFs of particle volume (P_D^v) and mass release rate (P_D^N) with respect to Taylor shape parameter D. For systems with particles of the same size, P_D^N is defined as,

$$P_D^N(t)\delta D = \frac{\delta(N_S')_{D\to D+\delta D}}{N_{S,tot}'(t)} \tag{20}$$

where $\delta(N_S')_{D\to D+\delta D}$ is the mass release rate of particles in the range from D to $D + \delta D$. Figure 8 shows the evolution of P_D^v and P_D^N for $C_{p,0}/C_s = 0.1$, 1, and 10. For all initial particle concentrations, the evolution of P_D^v demonstrates a similar pattern. Because the particle size reduction rate increases with increase in $|D|$, the initial horizontal straight line of P_D^v gradually decreases at both ends where $|D|$ is larger. At the same time, the middle area of the line where $|D|$ is small bulges upwards. With the faster size reduction and complete dissolution of particles of larger $|D|$, the upward bulge becomes narrower and the peak gets higher, until all particles are completely dissolved or the solution is saturated. As shown in the figure, the evolution of P_D^N of different $C_{p,0}/C_s$ demonstrates a similar pattern. According to Wang et al. [24], particles of larger $|D|$ have higher mass release rates (for the same particle size and bulk concentration). Therefore P_D^N is higher at both ends of the profile where $|D|$ is larger at the beginning ($t = 0$), forming a concave shape. With the faster dissolution of particles of larger $|D|$, the two ends of the profile fall and the middle rises, forming an upward bulge. As time goes on, the upward bulge becomes narrower and the peak rises. Comparison of the profiles of P_D^v and P_D^N shows that P_D^N has a wider profile, suggesting that the particles of

larger $|D|$ have a fraction of mass release rate (P_D^N) greater than their volume fraction (P_D^v). For systems of $C_{p,0}/C_s = 10$, the profiles of both P_D^v and P_D^N do not change obviously over time, but the evolution of the profiles presents the same trends as for $C_{p,0}/C_s = 0.1$ and 1.

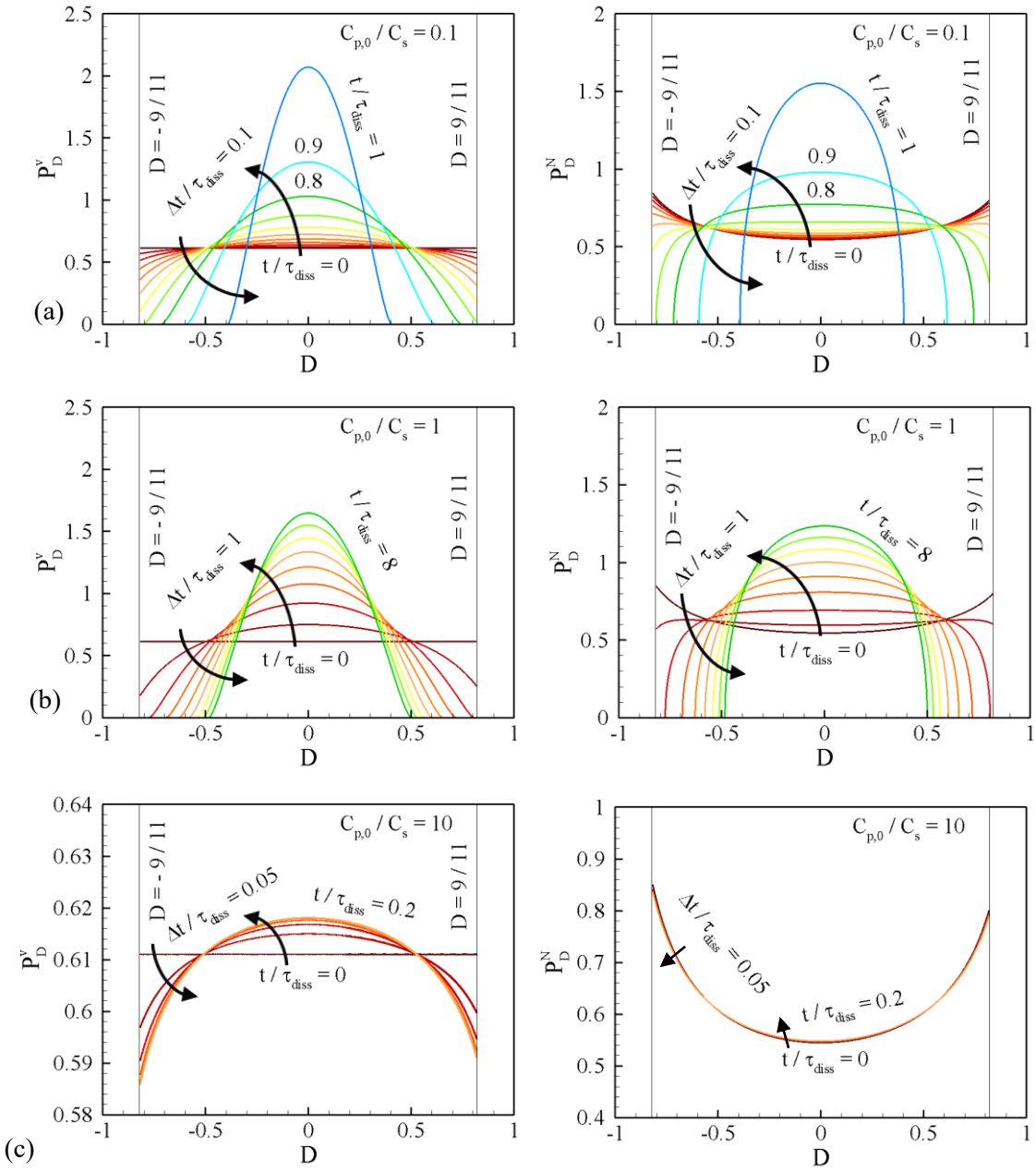

Figure 8. Evolution of particle size distribution (P_D^v) and mass release rate distribution (P_D^N) with respect to particle shape factor (D), in polydisperse systems of the same particle size. (a) $C_{p,0}/C_s = 0.1$, (b) $C_{p,0}/C_s = 1$, (c) $C_{p,0}/C_s = 10$. Left column: P_D^v, and right column P_D^N.

In Fig. 9, we compare the increase in bulk concentration (C_b/C_s) of polydisperse collections of particles of the same size but with a distribution of Taylor shape parameter, with monodisperse collections of particles. Three shape parameters $D = -9/11$, 0, and 9/11 are considered for the monodisperse collections. It is not surprising that for all $C_{p,0}/C_s$, the bulk concentration of polydisperse particles is higher than that

of monodisperse spherical particles ($D = 0$), but lower than that of monodisperse non-spherical particles ($D = -9/11$ and 9/11), at almost every moment. Since for the particles of smaller $|D|$, the mass release rates are close to that of spherical particles ($D = 0$) [24], the curves of C_b/C_s of polydisperse particles are close to the curves of monodisperse spherical particles, as shown in the figure.

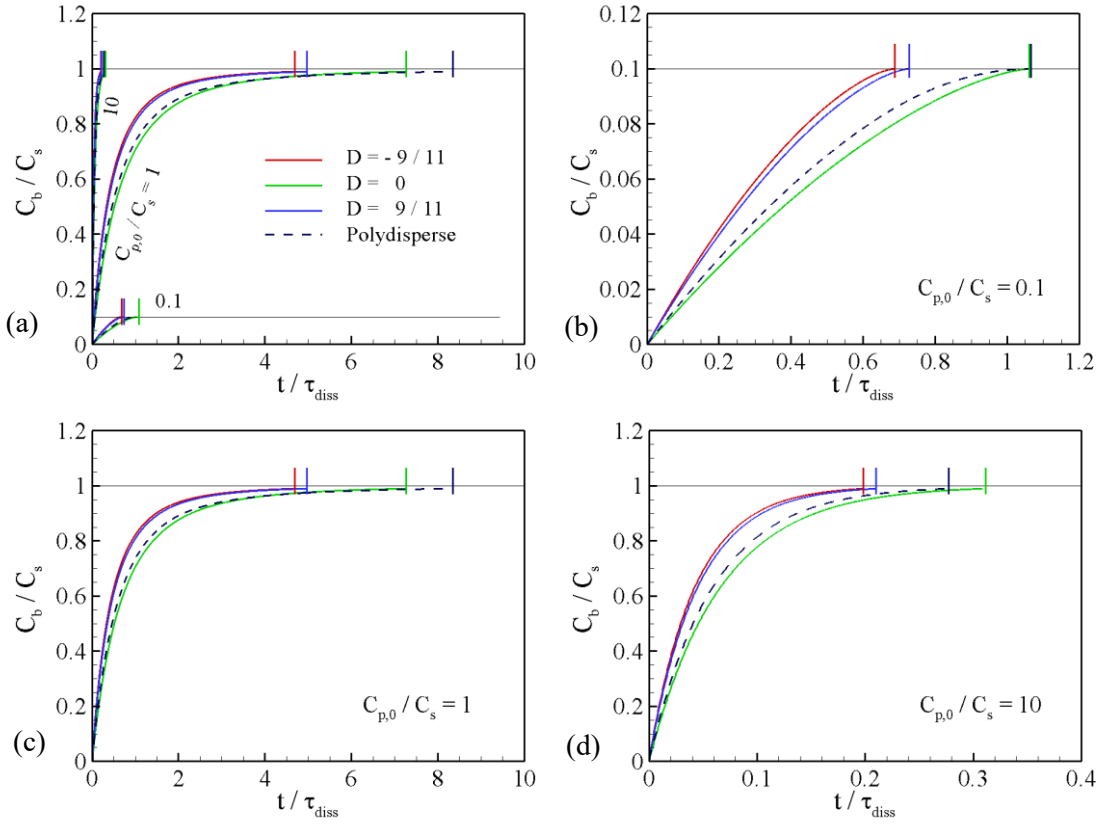

Figure 9. Variation of bulk concentration (C_b/C_s) of monodisperse collections of particles and polydisperse collections of particles of the same size but with a distribution of D. (a) Three initial particle concentrations: $C_{p,0}/C_s = 0.1$, 1 and 10, (b) $C_{p,0}/C_s = 0.1$, (c) $C_{p,0}/C_s = 1$, (d) $C_{p,0}/C_s = 10$.

Figure 10 shows the variation of dissolution time (T/τ_{diss}) of polydisperse collections of particles of the same size and three monodisperse collections of particles of different Taylor shape parameters ($D = -9/11$, 0, and 9/11). The initial particle concentration $C_{p,0}/C_s$ ranges from $C_{p,0}/C_s = 10^{-2}$ to 10^2. It can be seen in the figure that when $C_{p,0}/C_s < 1$, $log(T/\tau_{diss})$ of the polydisperse particles is very close to that of the monodisperse spherical particles. When $C_{p,0}/C_s$ is close to 1, $log(T/\tau_{diss})$ of the polydisperse particles is even larger than that of the monodisperse spherical particles. The faster dissolution of non-spherical particles does not decrease the dissolution time ($log(T/\tau_{diss})$) of the polydisperse systems, because the faster increase in bulk concentration caused by the dissolution of non-spherical particles of larger $|D|$ in the initial period of time suppresses the dissolution of spherical and nearly spherical particles. The dissolution of spherical and nearly spherical particles thus has to occur at relatively high bulk concentration, which causes the increase in $log(T/\tau_{diss})$ of the systems. When $C_{p,0}/C_s > 1$, the solution is saturated more by non-spherical particles of larger $|D|$. Therefore, the dissolution time $log(T/\tau_{diss})$ of polydisperse particles is lower than that of monodisperse spherical particles, but higher than monodisperse non-spherical particles.

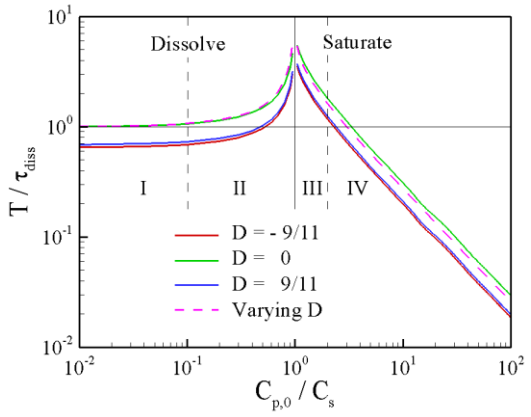

Figure 10. Variation of dissolution time (T/τ_{diss}) of monodisperse collections of particles and polydisperse collections of particles of the same size but with a distribution of Taylor shape parameter.

(c) Dissolution with initial particle distribution in both particle size and shape factor

For systems of spheroidal particles of various sizes and shapes, dissolution is influenced by the distributions of size and shape. Here we consider an ideal case, in which the initial particle volumetric PDF with respect to the logarithm of equivalent spherical radius $logR$ and Taylor shape parameter D is described by Eqn. (12). From the above discussion we have concluded that for particles of the same shape, smaller particles have larger size reduction rates, and for particles of the same size, particles of larger $|D|$ have larger size reduction rates. These two conclusions are also valid in the present complex systems. For brevity, the particle size reduction rate will not be discussed in this section. Three initial particle concentrations, $C_{p,0}/C_s = 0.1$, 1, and 10, are analyzed as examples of completely dissolved, exactly dissolved, and partially dissolved systems.

For systems with distributions of both particle size and particle shape, the PDF of mass release rate $P^N_{logR,D}$ is defined as,

$$P^N_{logR,D}(t)\delta(logR)dD = \frac{d(N'_S)_{logR\to logR+\delta(logR),D\to D+\delta D}}{N'_{S,tot}(t)} \tag{21}$$

where $(N'_S)_{logR\to logR+\delta(logR),D\to D+\delta D}$ is the mass release rate of particles in the range from $logR$ to $logR+\delta(logR)$ and from D to $D+\delta D$.

We start with a particle system with $C_{p,0}/C_s = 0.1$ and a wide initial particle size distribution. In Fig. 11 we plot the evolutions of volumetric PDF, $P^v_{logR,D}$, and PDF of mass release rate, $P^N_{logR,D}$, in the space of $log(R/R^*)$ and D, in the initial short period of time (from $t/\tau_{diss} = 0$ to 0.08). When $t/\tau_{diss} = 0$, the domain of particles is rectangular. $P^v_{logR,D}$ follows a log-normal distribution in the direction of $log(R/R^*)$ and remains constant in the direction of D. We have shown above that smaller particles have a greater mass release rate in the case of the same particle volume. This makes the distribution of $P^N_{logR,D}$ shift towards the small particle side relative to the distribution of $P^v_{logR,D}$, as shown in Fig. 11(b). Since particles of larger $|D|$ have a larger mass release rate, peaks of $P^N_{logR,D}$ are reached at the upper and lower ends of the distribution. After the dissolution starts, the motion of the boundaries of the iso-contours describes the changes in $log(R/R^*)$ and D of the particles at the boundaries of the particle domain. As noted by Wang et al. [24], the Taylor shape parameters of the particles do not change during the dissolution process, so the particles only participate in the movement to the left in the figure, that is, towards the small particle side. Due to the larger size reduction rates of the particles of smaller $log(R/R^*)$ and larger $|D|$, the upper and

lower ends of the left side of the domain extend to the left faster than the other areas, as shown in the figure. When $t/\tau_{diss} = 0.08$, all particles on the left boundary of the initial distribution have decreased in size to $log(R/R^*) < -5$. The distributions of larger magnitudes of $P^v_{logR,D}$ and $P^N_{logR,D}$ do not change much in this period.

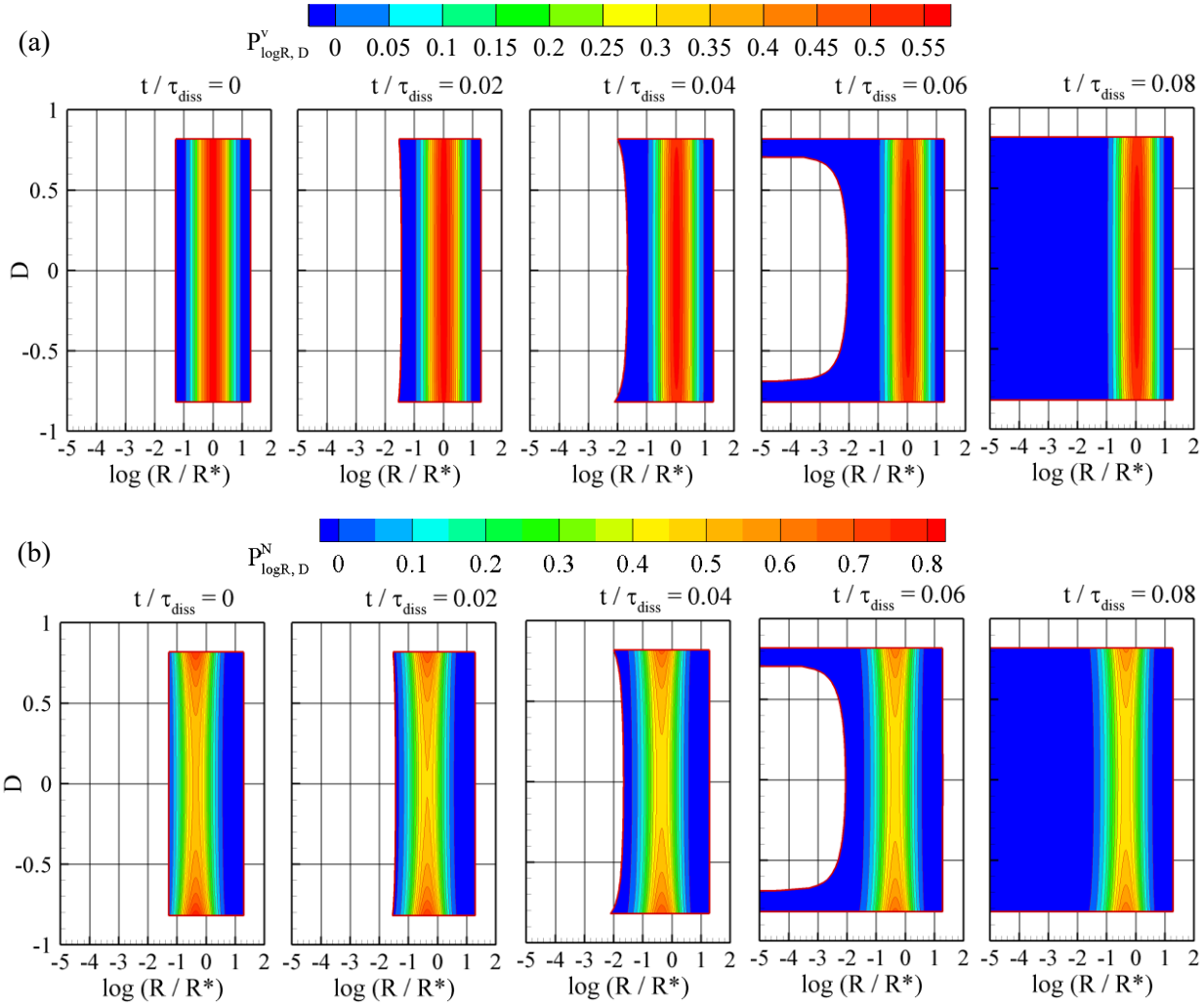

Figure 11. Initial evolution of particle size distribution ($P^v_{logR,D}$) and mass release rate distribution ($P^N_{logR,D}$) in the space of $log(R/R*)$ and D for $C_{p,0}/C_s = 0.1$. (a) $P^v_{logR,D}$, and (b) $P^N_{logR,D}$.

Figure 12 shows the evolution of $P^v_{logR,D}$, and $P^N_{logR,D}$ over a long period of time. Due to particle size reduction, the whole domain of the distributions moves toward the left. In this process, the patterns of the distributions change within the domain. Because of the larger size reduction rates of particles of larger $|D|$, the volumetric PDF, $P^v_{logR,D}$, decreases in the upper and lower regions and converges to the central region where $|D|$ is small. The non-uniform particle size reduction rate caused by the non-uniform distribution of D creates an arc curving to the left on the right boundary of the domain. At the same time, the faster size reduction rates of smaller particles cause the peak in the distribution of $P^v_{logR,D}$ to shift to the right, where it eventually reaches the right boundary. This is similar to the evolution of P^v_{logR} in systems in which all particles have the same shape (see Fig. 3). In the PDF of mass release rate, $P^N_{logR,D}$, the faster dissolution

rates of particles of larger $|D|$ make the peaks at the upper and lower boundaries of the initial distribution disappear quickly, and the distribution converges to the central region where $|D|$ is small. Due to the fast dissolution rates of smaller particles, the peak around $D = 0$ shifts to the large particle side in a fashion similar to that seen with $P^{v}_{logR,D}$.

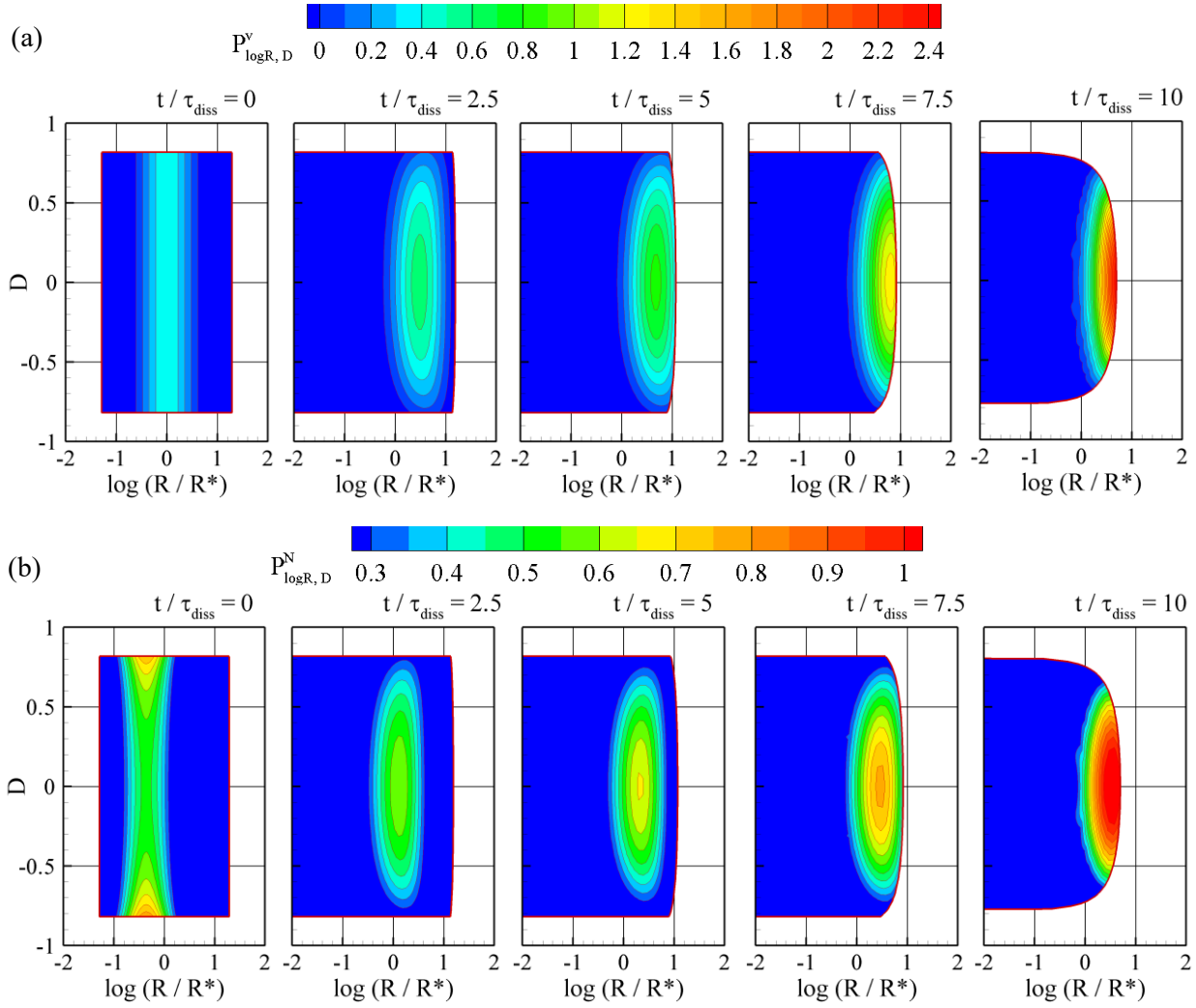

Figure 12. Long-period evolution of particle size distribution ($P^{v}_{logR,D}$) and mass release rate distribution ($P^{N}_{logR,D}$) in the space of $log(R/R^{*})$ and D for $C_{p,0}/C_s = 0.1$. (a) $P^{v}_{logR,D}$, and (b) $P^{N}_{logR,D}$.

For the cases with a narrow initial particle size distribution, the evolution of $P^{v}_{logR,D}$ and $P^{N}_{logR,D}$ is similar to those with a wide distribution, except that the peaks of $P^{v}_{logR,D}$ and $P^{N}_{logR,D}$ monotonically move to the left, like the evolution of P^{v}_{logR} in the systems of the same particle shape (Fig. 2). We will not go into detail on this topic here.

For the $C_{p,0}/C_s = 1$ cases, complete dissolution requires infinite time. The calculation was stopped at $C_b/C_s = 0.99$. Figure 13 shows the evolution of $P^{v}_{logR,D}$ in a system with a wide initial particle size distribution over the time period from $t/\tau_{diss} = 0$ to 100 for $C_{p,0}/C_s = 1$. When $t/\tau_{diss} = 100$, $C_b/C_s = 0.99$ is roughly reached. The non-uniform particle size reduction makes $P^{v}_{logR,D}$ converge to the central

region and move to the large particle side. At $t/\tau_{diss} = 100$, about 1% of the particle volume is left in the system, and the peak still has not reached the largest particles. This is similar to the cases with particles of the same shape (Fig. 4(b)).

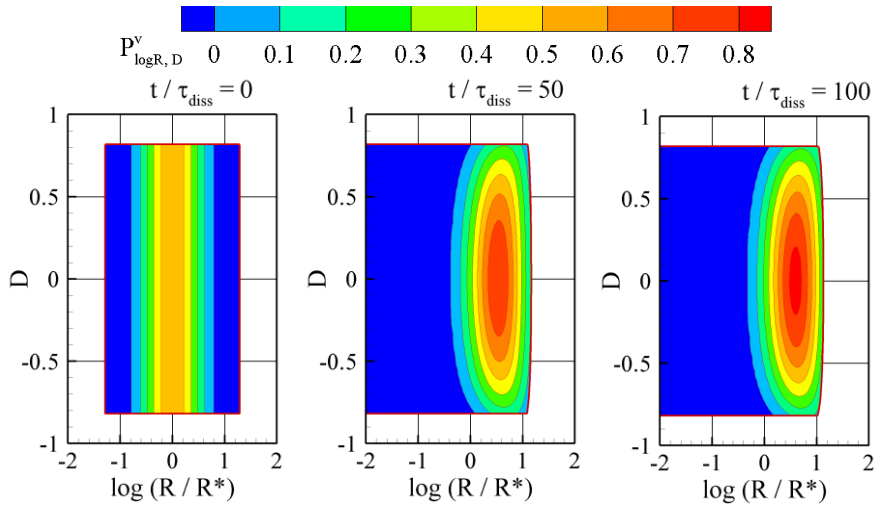

Figure 13. Evolution of particle size distribution ($P^v_{logR,D}$) in the space of $log(R/R*)$ and D for $C_{p,0}/C_s = 1$.

When $C_{p,0}/C_s = 10$, only 10% of the particle volume is dissolved in the solution when the process is complete, and the smaller particles play a more important role in the dissolution process. Figure 14 shows the evolution of $P^v_{logR,D}$ of a system with a wide initial size distribution for $C_{p,0}/C_s = 10$. When $t/\tau_{diss} = 0.2$, $C_b/C_s \approx 0.98$. As shown in the figure, the left boundary of the domain moves to the left, with larger extensions near the upper and bottom ends, due to the larger size reduction rates of particles of larger $|D|$. During the whole process, the distribution of $P^v_{logR,D}$ converges only slightly to the central region.

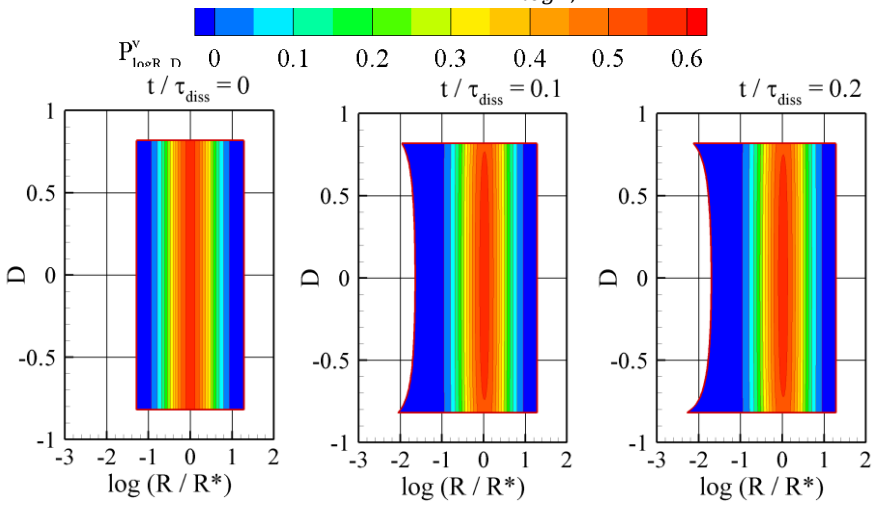

Figure 14. Evolution of particle size distribution ($P^v_{logR,D}$) in the space of $log(R/R^*)$ and D for $C_{p,0}/C_s = 10$.

In Fig. 15 we compare the increase in bulk concentration ($C_{b,0}/C_s$) of a polydisperse system with those of monodisperse systems for $C_{p,0}/C_s = 0.1$, 1, and 10. The Taylor shape parameters in the three monodisperse systems are $D = -9/11$, 0, and 9/11, respectively. A wide initial particle size distribution is used in the polydisperse systems. When $C_{p,0}/C_s = 0.1$ and 1, the faster dissolution of smaller particles and particles of large $|D|$ in polydisperse systems makes C_b/C_s increase in the initial short time period ($t/\tau_{diss} < 0.2$) at a rate close to that in monodisperse systems with $D = -9/11$ and 9/11. It's a coincidence that the increase rate of polydisperse systems is close to that of monodisperse systems. When we widen or narrow the initial distributions of the polydisperse particles, they will not be close to each other.

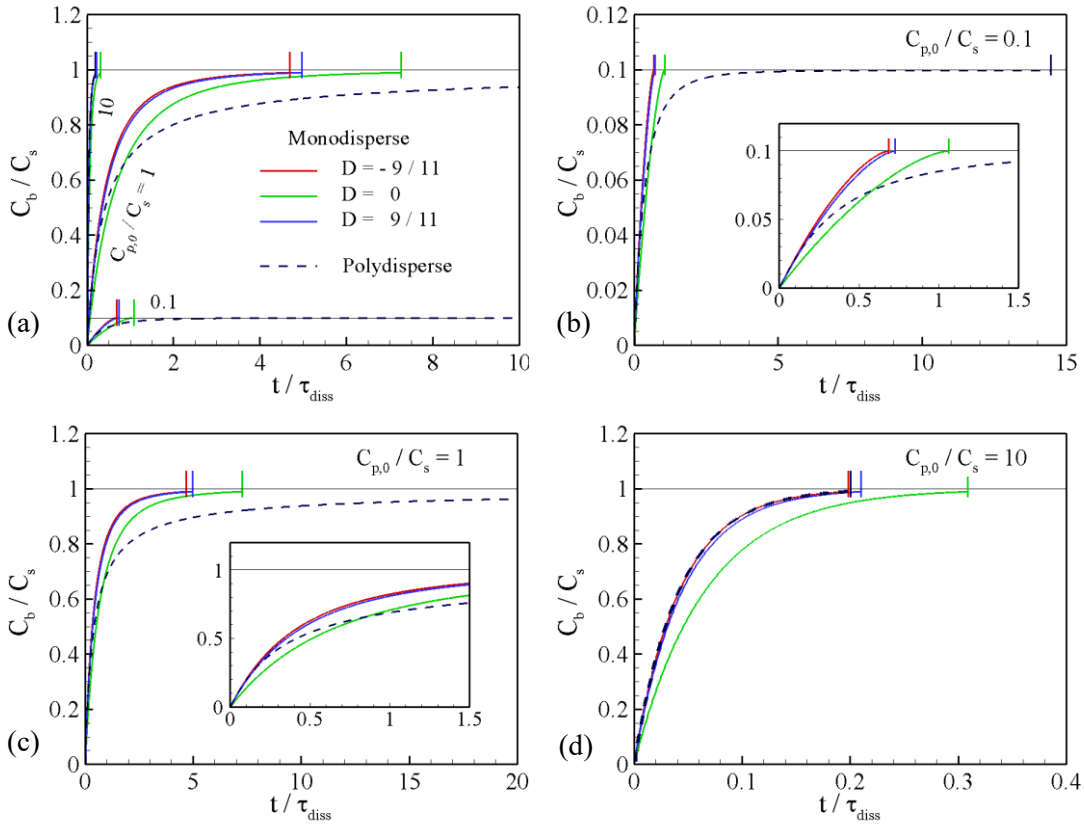

Figure 15. Variation of bulk concentration ($C_{p,0}/C_s$) with time (t/τ_{diss}) of monodisperse and polydisperse particles. (a) Three initial particle concentrations, $C_{p,0}/C_s = 0.1$, 1 and 10, (b) $C_{p,0}/C_s = 0.1$, (c) $C_{p,0}/C_s = 1$, (d) $C_{p,0}/C_s = 10$.

After the initial time period, the larger particles play a more important role, which significantly reduces the dissolution rate. As a result, the increase of C_b/C_s in polydisperse systems becomes slower than in any of the monodisperse systems. Correspondingly, the dissolution time in polydisperse systems becomes much longer than in monodisperse systems. If a further wider initial distribution is used, the bulk concentration will increase faster than in the current polydisperse system in the initial period and increase slower after that. When $C_{p,0}/C_s = 10$, the dissolution process is dominated by smaller particles in the polydisperse system, and the smaller particles have a larger dissolution rate. As a result, the bulk concentration increases at a rate close to that of monodisperse systems with $D = -9/11$ and 9/11. If the initial size distribution is further widened, C_b/C_s will increase even faster in the polydisperse system.

In Fig. 16, we compare the dissolution time, T/τ_{diss}, of polydisperse systems of both narrow and wide distributions with the dissolution time of monodisperse systems of different Taylor shape parameters, over the range from $C_{p,0}/C_s = 10^{-2}$ to 10^2. When $C_{p,0}/C_s < 1$, the dissolution time of the polydisperse systems is dominated by the largest particles in the systems. Because $(R_{0,max})_{wide} > (R_{0,max})_{narrow} > (R_{0,max})_{mono}$, we have $(\log(T/\tau_{diss}))_{wide} > (\log(T/\tau_{diss}))_{narrow} > (\log(T/\tau_{diss}))_{mono}$ for each $C_{p,0}/C_s$. When $C_{p,0}/C_s$ is slightly greater than 1, this relationship is still valid, because the largest particles still play an important role. However, when $C_{p,0}/C_s$ is further increased, so that the smaller particles play a more important role in the dissolution ($C_{p,0}/C_s > 3$ in the figure), the relationship will be changed. Because $(R_{0,min})_{wide} < (R_{0,min})_{narrow}$, the dissolution time of the polydisperse systems of a wide initial

size distribution becomes smaller than that of a narrow distribution for each $C_{p,0}/C_s$. It is apparent that the dissolution time of polydisperse systems is smaller than that of monodisperse spherical particle systems. Nevertheless, the comparison of T/τ_{diss} between polydisperse systems and monodisperse systems of non-spherical particles depends on the initial size distribution of the polydisperse systems and the Taylor shape parameters of the monodisperse systems.

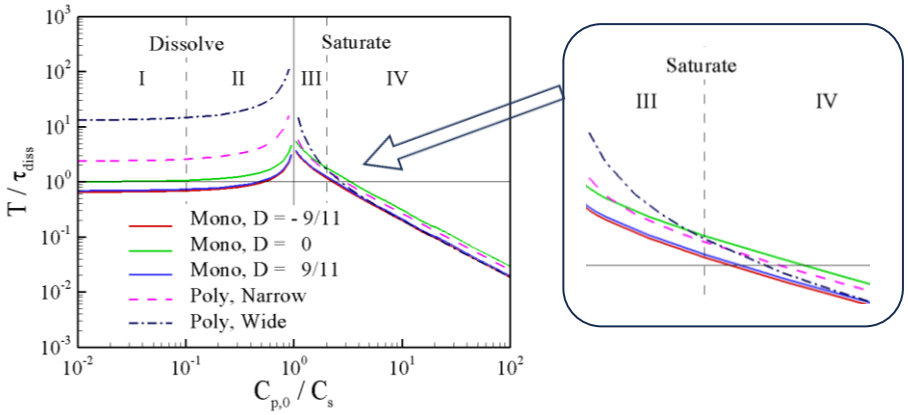

Figure 16. Variation of dissolution time (T/τ_{diss}) with initial concentration of solid particles ($C_{p,0}/C_s$) between monodisperse and polydisperse particles.

3. Conclusion

Using the polydisperse dissolution model developed in Part I of this study, we conducted a systematic investigation into the dissolution characteristics of typical polydisperse spheroidal particle systems. The effects of the distributions of particle size and shape have been studied by examining detailed dissolution processes, such as the size reduction rates of individual particles, the increase in bulk concentration, and the dissolution time of the polydisperse systems. Some important factors controlling the dissolution details, including initial particle concentration, the smallest and largest particle sizes, and the smallest and largest Taylor shape parameters of particle shapes, have been identified.

The diversity of particle sizes and shapes in polydisperse systems causes non-uniform dissolution, in terms of mass release rate and particle size reduction rate of individual particles, leading to completely different dissolution characteristics from monodisperse systems. Notably, under conditions of the same bulk concentration and particle volume, smaller particles have larger size reduction rates and greater mass release rates. Under the condition of the same particle size, particles with a larger deviation from spherical shape (represented by the absolute value of the Taylor shape parameter) have larger size reduction rates and greater mass release rates. Governed by these two principles, when the initial particle concentration is lower than the saturation concentration, particles of smaller sizes and larger deviation from spherical shape dominate the initial stage of the dissolution process, while particles of larger sizes and smaller deviation from spherical shape take over in the later stage. When the initial particle concentration is higher than the saturation concentration, the overall dissolution process is primarily dominated by particles of smaller sizes and greater deviation from spherical shape throughout. The distribution of particle sizes and shapes, especially the minimum and maximum particle sizes and Taylor shape parameters, play an important role in determining the detailed dissolution process.

These principles and findings establish a crucial foundation for actively managing the dissolution of polydisperse particle systems. They can be adapted for use in a broad spectrum of irregular particle systems with appropriate adjustment.

Data accessibility. The data that support the findings of this study are available from the corresponding author upon reasonable request.

Competing interests. We declare that we have no competing interests.

Funding. This work was supported by the National Science Foundation (Award ID: 2138740)

References[ ]

[1] Salehi, N., Al-Gousous, J., Mudie, D.M., Amidon, G.L., Ziff, R.M. & Amidon, G.E. 2020 Hierarchical mass transfer analysis of drug particle dissolution, highlighting the hydrodynamics, pH, particle size, and buffer effects for the dissolution of ionizable and nonionizable drugs in a compendial dissolution vessel. *Molecular Pharmaceutics* **17**, 3870-3884.
[2] Petersen, J. 2016 Heap leaching as a key technology for recovery of values from low-grade ores–A brief overview. *Hydrometallurgy* **165**, 206-212.
[3] Badgujar, K.C. & Bhanage, B.M. 2015 Factors governing dissolution process of lignocellulosic biomass in ionic liquid: Current status, overview and challenges. *Bioresource technology* **178**, 2-18.
[4] Chamolly, A. & Lauga, E. 2019 Stochastic dynamics of dissolving active particles. *The European Physical Journal E* **42**, 1-15.
[5] Sheng, J.J., Sirois, P.J., Dressman, J.B. & Amidon, G.L. 2008 Particle diffusional layer thickness in a USP dissolution apparatus II: a combined function of particle size and paddle speed. *Journal of Pharmaceutical Sciences* **97**, 4815-4829.
[6] Hörter, D. & Dressman, J. 2001 Influence of physicochemical properties on dissolution of drugs in the gastrointestinal tract. *Advanced drug delivery reviews* **46**, 75-87.
[7] Jambhekar, S.S. & Breen, P.J. 2013 Drug dissolution: significance of physicochemical properties and physiological conditions. *Drug Discovery Today* **18**, 1173-1184.
[8] Wang, Y. & Brasseur, J.G. 2019 Enhancement of mass transfer from particles by local shear‐rate and correlations with application to drug dissolution. *AIChE Journal* **65**, e16617.
[9] Costa, P. & Lobo, J.M.S. 2001 Modeling and comparison of dissolution profiles. *European journal of pharmaceutical sciences* **13**, 123-133.
[10] Dali, M. 1999 Determination of mass transfer dissolution rate constants from critical time of dissolution of a powder sample. *Pharmaceutical development and technology* **4**, 1-8.
[11] Wang, J. & Flanagan, D.R. 1999 General solution for diffusion‐controlled dissolution of spherical particles. 1. Theory. *Journal of Pharmaceutical Sciences* **88**, 731-738.
[12] Wang, J. & Flanagan, D.R. 2002 General solution for diffusion‐controlled dissolution of spherical particles. 2. Evaluation of experimental data. *Journal of Pharmaceutical Sciences* **91**, 534-542.
[13] Shan, G., Igarashi, K. & Ooshima, H. 2002 Dissolution kinetics of crystals in suspension and its application to L-aspartic acid crystals. *Chemical Engineering Journal* **88**, 53-58.
[14] Hintz, R.J. & Johnson, K.C. 1989 The effect of particle size distribution on dissolution rate and oral absorption. *International journal of pharmaceutics* **51**, 9-17.
[15] Lu, A.T., Frisella, M.E. & Johnson, K.C. 1993 Dissolution modeling: factors affecting the dissolution rates of polydisperse powders. *Pharmaceutical research* **10**, 1308-1314.

[16] Johnson, K.C. 2003 Dissolution and absorption modeling: model expansion to simulate the effects of precipitation, water absorption, longitudinally changing intestinal permeability, and controlled release on drug absorption. *Drug development and industrial pharmacy* **29**, 833-842.
[17] Johnson, K.C. 2012 Comparison of methods for predicting dissolution and the theoretical implications of particle-size-dependent solubility. *Journal of Pharmaceutical Sciences* **101**, 681-689.
[18] Simöes, S., de Almeida, L.P. & Figueiredo, M. 1996 Testing the applicability of classical diffusional models to polydisperse systems. *International journal of pharmaceutics* **139**, 169-176.
[19] De Almeida, L.P., Simões, S., Brito, P., Portugal, A. & Figueiredo, M. 1997 Modeling dissolution of sparingly soluble multisized powders. *Journal of Pharmaceutical Sciences* **86**, 726-732.
[20] Zhong, W., Yu, A., Zhou, G., Xie, J. & Zhang, H. 2016 CFD simulation of dense particulate reaction system: Approaches, recent advances and applications. *Chemical Engineering Science* **140**, 16-43.
[21] Zhong, W., Yu, A., Liu, X., Tong, Z. & Zhang, H. 2016 DEM/CFD-DEM modelling of non-spherical particulate systems: theoretical developments and applications. *Powder technology* **302**, 108-152.
[22] Dali, M.V. & Carstensen, J. 1996 Effect of change in shape factor of a single crystal on its dissolution behavior. *Pharmaceutical research* **13**, 155-162.
[23] Sugano, K. 2010 Aqueous boundary layers related to oral absorption of a drug: from dissolution of a drug to carrier mediated transport and intestinal wall metabolism. *Molecular pharmaceutics* **7**, 1362-1373.
[24] Wang, Y., Wan, H., Wei, T., Nevares, D. & Shu, F. 2022 Quasi-steady-state modelling and characterization of diffusion-controlled dissolution from monodisperse prolate and oblate spheroidal particles. *Proceedings of the Royal Society A* **478**, 20220283.
[25] Wang, Y., Wan, H., Refuaiti, R., Wei, T., Shu, F. 2024 Quasi Steady-State Modeling and Characterization of Diffusion-Controlled Dissolution from Polydisperse Spheroidal Particles, I: Modeling. *Proceedings of the Royal Society A.*
[26] Lindfors, L., Jonsson, M., Weibull, E., Brasseur, J.G. & Abrahamsson, B. 2015 Hydrodynamic effects on drug dissolution and deaggregation in the small intestine—a study with felodipine as a model drug. *Journal of Pharmaceutical Sciences* **104**, 2969-2976.
[27] Heintzenberg, J. 1994 Properties of the log-normal particle size distribution. *Aerosol Science and Technology* **21**, 46-48.
[28] Bergmann, R.B., Shi, F.G., Queisser, H.J. & Krinke, J. 1998 Formation of polycrystalline silicon with log-normal grain size distribution. *Applied surface science* **123**, 376-380.
[29] Wang, Y., Abrahamsson, B., Lindfors, L. & Brasseur, J.G. 2012 Comparison and analysis of theoretical models for diffusion-controlled dissolution. *Molecular Pharmaceutics* **9**, 1052-1066.